Title

Microliter ultrafast centrifuge platform for size-based particle and cell separation and extraction using novel omnidirectional spiral surface acoustic waves

Journal

Lab on a Chip, 21(5)

ISSN

1473-0197

Authors

Zhang, Naiqing
Zuniga-Hertz, Juan P
Zhang, Elizabeth Yan
et al.

Publication Date

2021-03-07

DOI

10.1039/d0lc01012j

Peer reviewed

Journal Name

ARTICLE TYPE

Cite this: DOI: 00.0000/xxxxxxxxxx

Microliter ultrafast centrifuge platform for size-based particle and cell separation and extraction using novel omnidirectional spiral surface acoustic waves†

Naiqing Zhang [a], Juan P. Zuniga-Hertz [b], Elizabeth Yan Zhang [d], Tilvawala Gopesh [a], Mckenzie J. Fannon [b], Jiaying Wang [c], Yue Wen [a], Hemal H. Patel [b], and James Friend*[a]

Received Date
Accepted Date

DOI: 00.0000/xxxxxxxxxx

Asymmetric surface acoustic waves have been shown useful in separating particles and cells in many microfluidics designs, mostly notably sessile microdroplets. However, no one has successfully extracted target particles or cells for later use from such samples. We present a novel omnidirectional spiral surface acoustic wave (OSSAW) design that exploits a new cut of lithium niobate, 152 Y-rotated, to rapidly rotate a microliter sessile drop to $\sim 10g$, producing efficient multi-size particle separation. We further extract the separated particles for the first time, demonstrating the ability to target specific particles, for example, platelets from mouse blood for further integrated point-of-care diagnostics. Within $\sim$5 s of surface acoustic wave actuation, particles with diameter of 5 μm and 1 μm can be separated into two portions with a purity of 83% and 97%, respectively. Red blood cells and platelets within mouse blood are further demonstrated to be separated with a purity of 93% and 84%, respectively. These advancements potentially provide an effective platform for whole blood separation and point-of-care diagnostics without need for micro or nanoscale fluidic enclosures.

1 Introduction

Surface acoustic wave devices have become popular as a practical and effective tool for fluid manipulation, particle and cell sorting and separation, and fluid jetting and atomization in various acoustofluidics and biomedical applications in recent years [1–6]. They offer substantial energy density in 40–100 MHz high-frequency, short-wavelength acoustic waves, providing useful acoustofluidic effects when coupled with liquid [7–9]. Due to various acoustic radiation forces exerted on particles and cells of different sizes and properties, rapid separation of particles and cells in liquid media using SAW has been one of the most popular and effective methods in microscale acoustofluidics applications for biomedical diagnostics [10,11]. SAW-based separation in enclosed channels has produced high throughput needed in practical applications [12,13]. Traveling surface acoustic waves (TSAW) and standing acoustic waves (SSAW) have both been used to continuously separate particles and cells based on their size and mechanical properties [14–19]. However, the need for a microchannel fabrication process and a syringe pump to complete the separation and provide a method of extraction complicates the system and renders its use in a clinical setting problematic, especially when the cost of single-use sterile microchannels are considered. Another SAW-based separation technique is to place a sessile microliter liquid drop on top of the piezoelectric substrate where SAW is generated, passing sound into the drop, in turn producing rapid separation of particles and cells within [20,21]. This simple method does not require an external pumping system nor a sophisticated channel fabrication and bonding process. Since only a microliter sample is required—a mere pinprick of blood, for example—the method is potentially quite convenient for clinical use. The potential for sterile sample testing using a superstrate [22] improves the likelihood of eventual clinical use.

Importantly, none of these past approaches have actually *extracted* the separated components from the sessile drop after centrifugation, a key problem in the technique's future use. Bourquin *et al.* [23] presented enrichment of malaria-infected red blood cells

[a] *Center for Medical Devices and Instrumentation, Department of Mechanical and Aerospace Engineering, University of California San Diego, CA 92093, USA.*
[b] *Department of Anesthesiology, U.S. Veterans Administration, San Diego Healthcare System, University of California San Diego, CA 92093, USA.*
[c] *Department of NanoEngineering, University of California San Diego, CA 92093, USA.*
[d] *Rady School of Management, University of California San Diego, CA 92093, USA.*
E-mail: jfriend@eng.ucsd.edu; Tel: +(858) 534 3781

† Electronic Supplementary Information (ESI) available: Videos of the displacement field induced by the spiral interdigital electrode, and a demonstration of particle and blood separation. See DOI: 10.1039/b000000x/

at periphery of the droplet based on density difference using SAW-induced separation in sessile drop, enabling effective detection directly from the droplet, and many of the references in this introduction describe various methods for separating particle and cell components in a sessile drop in a similar way. However, after shutting off the acoustic wave, diffusion slowly recombines the components, destroying the separation.

For most point-of-care diagnostics and biomedical applications, further analysis and integrated tests of separated samples are necessary. There remains a need to centrifuge a sessile drop, separate cell or particle components in that drop based on size, acoustic properties, or both, and enable an efficient *extraction* of target cells or particles from the sessile drop sample. In this paper, a method for centrifugation of a sessile drop and extraction of particles and cells from that drop is described.

It is important to first, however, point out an important part of piezoelectric material choices and electrode design to enable sessile drop centrifugation. In the last decade, straight interdigital transducers (IDTs) with a sessile drop asymmetrically located at the edge of the SAW propagation (aperture) producing spinning of the drop and particle concentration and separation within[20,24]. Different acoustic radiation and centrifugal forces based on particle sizes and mechanical properties have been utilized to perform temporary separation in this arrangement. Destgeer *et al.* [21] suggested in a later study that four distinct regimes of particle concentration exist in a sessile drop under asymmetric SAW actuation. Focusing IDTs have been used to locally enhance the SAW intensity to improve sessile drop spinning, with some consideration of the focused shape of the IDT[25]. However, anisotropic substrates, the difficulty in repeatedly and accurately placing sessile drops, and large energy losses because of the offset position reduce the attractiveness of this approach with straight or focusing IDTs.

For a rather different purpose, an annular IDT has been demonstrated to generate focusing SAW from all directions to a single, diffraction-limited spot[26]. The IDT finger shape was designed based on the slowness curve of SAW propagating across anisotropic LN so that the generated surface acoustic waves converge to a small spot at the center of the transducer, limited only by diffraction. However, this IDT design simply focuses energy at one spot, without the necessary asymmetry to generate fluid spinning in the droplet and consequent particle separation. There has, in the past few years, been a flood of interest in locally generated torsional waves in fluids by either an array of radially placed IDTs or weak spiral IDT structures to produce particle entrapment[27]. While all these works are excellent, they do not address the fact that, in the most widely used cut of LN today in acoustofluidics and telecommunications, 127.86 Y-rotated LN, the piezoelectric coupling is an order of magnitude less along the Y axis of the substrate compared to the X axis, producing a far weaker SAW in the Y direction. Other choices are possible, including zinc oxide[28] and aluminum nitride[29], but these thin-film materials are generally limited to 2 μm or less thickness and have relatively poor piezoelectric coupling coefficients, making them poor by comparison to single crystal, bulk LN for high-power applications such as acoustofluidics. Lead zirconate titanate (PZT) is another popular polycrystalline choice, but is not only toxic with elemental lead present in the interstitial grain boundaries that can easily contaminate a fluid sample, it also is lossy and rapidly heats, especially at high frequencies.

Rather than relying on an asymmetric technique, arguably a better approach to spinning a sessile drop would be to have SAW propagate inwards from all directions, tangentially converging to a circle of defined diameter equal to or smaller than the drop size to produce a net moment about a vertical axis. Using this idea, we conceive an axisymmetric, omnidirectional spiral SAW to induce planar recirculating acoustic streaming in a droplet, causing its rapid rotation. We exploit a recent discovery of a different cut of LN, 152° Y-rotated LN[30] that is able to support SAW in an arbitrary direction with nearly the same piezoelectric coupling and other relevant material properties. Combining the choice of this material and our unusual IDT design produces a result that enables rapid sessile drop rotation sufficient to produce centrifugation superior to past results.

2 Concept and Design

A unique spiral IDT design underpins our effort to generate rotational symmetric SAW in a central circular region so that energy can be efficiently transferred into the sessile drop for improved fluid spinning and consequent particle and cell separation. The SAW at any point generated by the spiral IDT is designed to propagate along a constant offset angle relative to its radial direction, α, into the middle circular region. The spiral equation in polar coordinates (r,θ) to produce the spiral IDT of the OSSAW is (see details of the derivation in the Appendix):

$$\theta = \sqrt{\frac{r^2}{R_0^2}-1} - \tan^{-1}\sqrt{\frac{r^2}{R_0^2}-1} - \sqrt{\frac{R_1^2}{R_0^2}-1} + \tan^{-1}\sqrt{\frac{R_1^2}{R_0^2}-1}. \quad (1)$$

where R_0, R_1, and R_2 are the radii of circles that define the tangent circle for the inward propagating SAW, the outer edge of the spiral IDT, and the inner edge of the spiral IDT, respectively, as illustrated in Fig. 1.

The omnidirectional spiral design is obtained by azimuthally shifting and duplicating a single finger pair to produce the complete set of IDT fingers (*see* Fig. 1). The number of duplications required in this simple IDT format is determined by an equality between the finger width, the gap between them, and one quarter of a wavelength. We have

$$R_2\frac{2\pi}{n}\sin\alpha = \frac{\lambda}{4} = \frac{v}{4f}, \quad (2)$$

where R_2 is the inner radius of the spiral IDT; $n/2$ is the number of spiral IDT fingers; α is the offset angle for SAW propagation; λ, f, v are wavelength, frequency, and phase velocity of surface acoustic wave propagating on LN respectively. This simplifies to

$$n = \frac{8\pi f R_2 \sin\alpha}{v} \quad (3)$$

where the number of spiral lines n are dependent on the wave frequency f, radius of inner circle of spiral IDTs R_2, SAW offset angle α, and SAW phase velocity v.

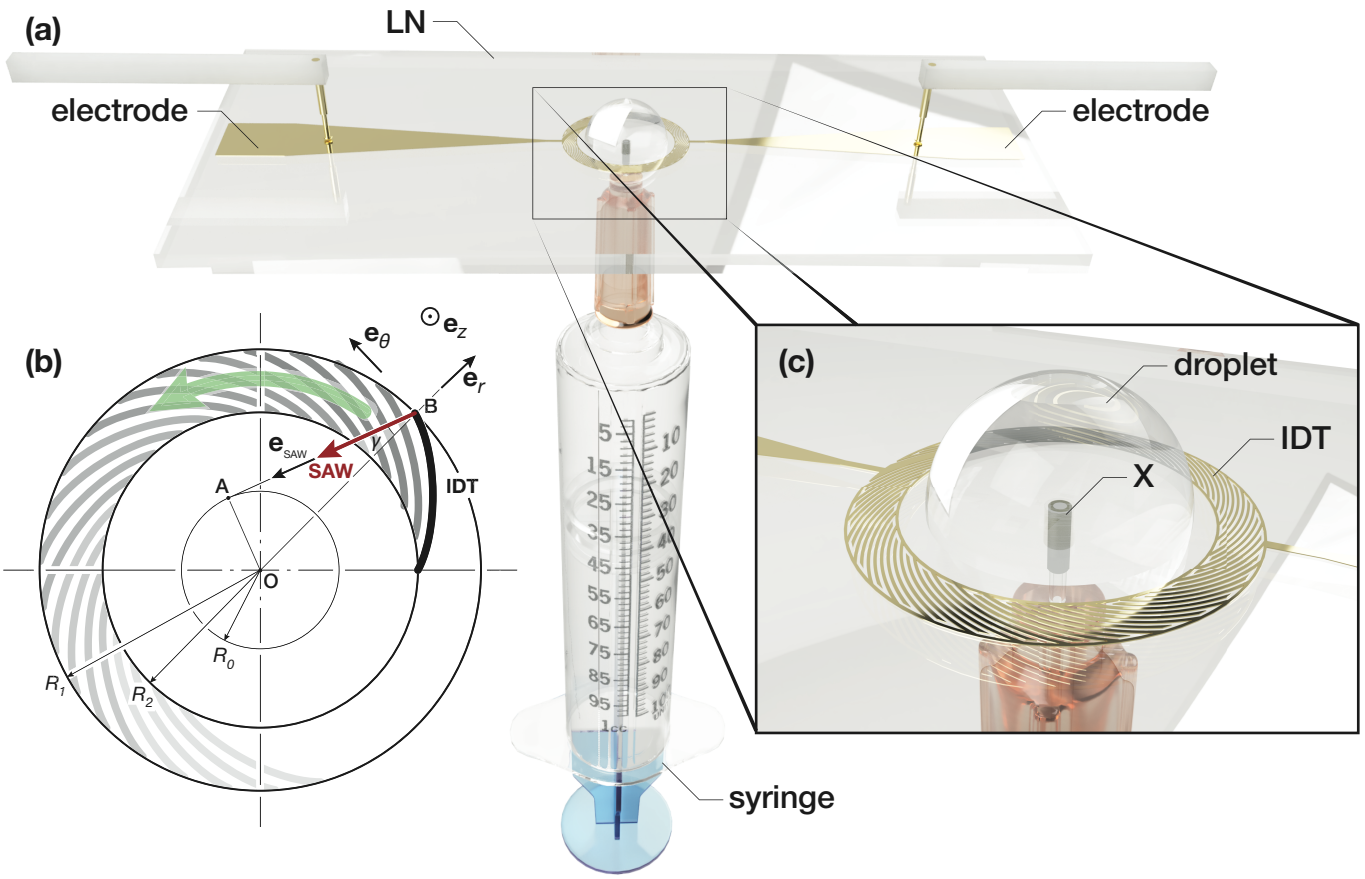

Fig. 1 The (a) omnidirectional spiral surface acoustic wave (OSSAW) device concept for centrifugation and separation of samples, based on (b) the use of a spiral interdigital electrode structure defined in detail in the Appendix, an extraction syringe, and a 152° Y-rotated cut of lithium niobate to allow SAW to be generated along the substrate surface. The bold spiral line represents the spiral IDT finger; the red arrow represents the SAW it generates from the outer end of the finger, propagating inwards. The outward propagating SAW is absorbed with polymer absorbers (not shown for clarity). The SAW propagating direction is orthogonal to the spiral line and tangent to a defined circle of radius R_0. The IDT fingers are defined between the outer and inner radii R_1 and R_2. A closer view (c) of the OSSAW electrode with a $\mu\ell$-order droplet within shows the spiral IDT, the bus bars that connect, independently, the inner and outer fingers of the IDT, with an independent connection from the outside to the inner bus bar at left in the closeup, and the (X) location of the laser-drilled hole used for extraction after centrifugation.

Crucially, in this concept the in-plane anisotropy of the piezoelectric substrate is not considered. We are able to make this remarkable assumption by using a new cut of LN, the 152° Y-rotated (152Y) LN cut, instead of the conventional 128° Y-rotated cut. This new cut has been shown through an exhaustive analysis to be an optimal choice to simultaneously minimize in-plane anisotropy and maximize electromechanical coupling for omnidirectional surface acoustic wave propagation[30]. The combination of this cut with the spiral design facilitates the type of azimuthally distributed SAW important in enhancing the sessile drop rotation through more intense acoustic streaming and acoustic radiation force via coupling from all propagation directions. An alternative approach would be to reshape the spiral electrode pattern in order to match the "slowness curve" and best make use of an existing anisotropic cut of lithium niobate like the 128° Y-rotated cut[26]. However, this does not overcome the poor electromechanical coupling of any acoustic wave away from the X axis in that cut, and indeed in most other cuts of LN.

3 Device fabrication and functionality

3.1 Device fabrication

Equation (1) was discretized into points, equally spaced at 1 μm, along a single spiral line (MATLAB, Mathworks, Natick, MA USA), and formed into a complete array using computer-aided drafting (AutoCAD, Autodesk, San Rafael, CA, USA) according to the number of spiral lines, n in Eqn. (3), as defined and fabricated for three different operating frequencies of 40 MHz, 56.5 MHz, and 100 MHz, later shown to be useful for choosing the threshold size for particle separation within the sessile droplet. An operating frequency of 56.5 MHz was chosen to produce a ~5 μm particle/cell separation threshold, taking into account particle compressibility[31–33], by designing the spiral IDT electrode to operate with a wavelength of $\lambda \sim 70$ μm (from $f = v/\lambda$). A polymer mask was produced (CAD/Art Services, Inc., Bandon, OR USA) from this result. Standard UV photolithography (using AZ1512 photoresist and AZ300MIF developer, MicroChem, Westborough, MA USA) was used alongside sputter deposition and lift-off processes

to fabricate the 5 nm Cr/ 400 nm Au IDT upon a 500 μm-thick, double-polished 152Y LN substrate (Jiaozuo Commercial FineWin Co., Ltd, Jiaozuo, Henan, China)[1,34,35]. The whole wafer was diced into fifteen 26.7 mm $\times$ 12 mm LN chips (Disco Automatic Dicing Saw 3220, Disco Corporation, Tokyo, Japan). Absorbers (DragonSkin, platinum-cure silicone rubber, Smooth-On, Inc., Macungie, PA, USA) were used at the periphery of the device to prevent edge reflections and spurious bulk waves. SAW was generated by applying a sinusoidal electric field to the IDT at resonance using a signal generator (WF1967 multifunction generator, NF Corporation, Yokohama, Japan) and amplifier (ZHL–1–2W–S+, Mini-Circuits, Brooklyn, NY USA). The instantaneous voltage and current were measured and used to compute the true power input on an oscilloscope (InfiniiVision 2000 X-Series, Keysight Technologies, Santa Rosa, CA USA). The spatiotemporal variations of the SAW displacement and velocity amplitude along the underlying substrate were measured using a laser Doppler vibrometer (LDV, UHF–120, Polytec, Waldbronn, Germany).

3.2 Wave morphology

Surface acoustic waves propagating inward from the OSSAW spiral structure may pass through the center and outward to interfere with SAW from the opposite side, unless a fluid droplet is present to "leak" and absorb the acoustic wave in the substrate[36] before this can happen. This is a key design parameter in selecting the frequency of the SAW and the inner diameter of the OSSAW structure, R_2. It also defines the fluid sample size, because the sessile drop must both fit within the inner diameter of this spiral ring IDT and completely occupy the space to ensure complete absorption of the SAW from the substrate.

In other words, the sample volume defines the appropriate frequency to choose for the SAW device, presuming the contact angle does not change significantly. If another fluid sample volume is desired, the design of the IDT should change to provide a matching frequency so that complete attenuation occurs.

In our case, the attenuation length of the SAW in the substrate underneath a fluid is $\alpha^{-1} = (\rho_s v_R \lambda_{SAW})/(\rho_f c_f) \sim$0.9 mm, where ρ_s and ρ_f are the density of LN and water, v_R is the velocity of the SAW on the LN substrate, and c_f is the sound velocity in water[9], respectively. Upon positioning a 1.5 $\mu\ell$ drop in the middle of the device with a radius of 1 mm, SAW from the opposite direction is absorbed by the liquid, eliminating possible interference.

To confirm this concept, a diced OSSAW device including a spiral IDT of inner radius $R_2 = 0.5$ mm was scanned via LDV; a video of the result is provided as Electronic Supplementary Information (ESI)†. A small drop of DragonSkin silicone rubber was placed and cured in the middle of the inner region of the device as a direct substitute for a fluid droplet. This absorbs the SAW propagating from the opposite side of the device in a manner similar to a water or other fluid drop, but does not evaporate nor change shape during the scan. The spatial phase distribution is plotted in Fig. 2(a) while being driven at 2.6 W and 56.5 MHz. The phase pattern indicates an inward propagating SAW at an oblique angle as desired, though there are discrepancies in the axisymmetry of the wave morphology.

The ability to generate SAW along directions away from the X axis is significantly better in this 152° Y-rotated cut LN than 127.86° Y-rotated LN. Both the speed of sound and the electromechanical coupling, on average, change much less than with the 127.86° Y-rotated cut popular for unidirectional X-axis propagating SAW. It is impossible to completely eliminate in-plane anisotropy without also eliminating the piezoelectric coupling necessary to efficiently generate SAW across the plane of the surface. This is why Z-cut and X-cut LN, both isotropic in the plane of the surface, are poor choices for SAW generation. The details of the analysis that produces the 152° Y-rotated cut as an optimal choice are provided in the literature[30], as is information on why the anisotropy is necessary.

The rather broad resonance frequency exhibits a peak at 56.5 MHz as shown in the frequency response plot in Fig. 2(b).

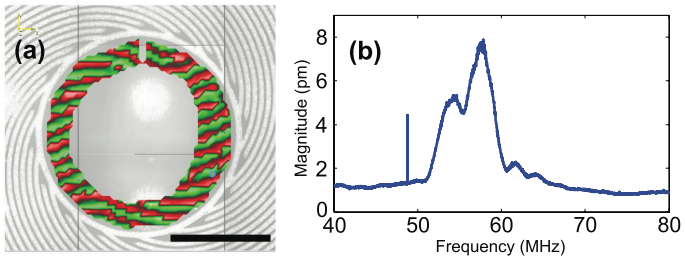

Fig. 2 (a) An LDV phase scan of the OSSAW inner annular region, showing inward, obliquely propagating waves (scale bar: 0.5 mm). (b) The OSSAW device exhibits a resonance at 56.5 MHz according to the LDV-measured frequency spectrum. Note: the peculiar "notch" at the top of each image is due to a strange limitation in the LDV software: a measurement cannot be made in a complete annular region; it must be broken.

3.3 OSSAW Droplet Spinning Functionality

The key purpose of the OSSAW design is to enhance the ability to spin sessile microliter-scale fluid droplets, as investigated here. A method to form an aligned and precisely sized wetting region has been devised for this purpose. It is important to accurately place the droplet at the center of the OSSAW structure with cylindrical symmetry. Doing so without surface modification, whether by hand or machine, is difficult. The entire surface of the OSSAW substrate was coated with a hydrophobic submicron film (Aquapel, Pittsburgh, PA USA). A precise circular region of $R_2 = 0.5$ mm radius was etched by an excimer (exciplex) laser ($\lambda = 189$ nm, firing rate of 40 Hz, power of 0.16 W, and 5 shots, LaserShot, Optec, Frameries Belgium). The weak and brief laser machining acted to remove this coating from the region, returning it to the naturally hydrophilic state of bare, polished LN without damage. This enables repeatable and precise droplet placement—even by hand with a standard pipette.

It is important to examine how the acoustic streaming-driven flow evolves when using the OSSAW device, and a useful comparison is the traditional placement of a fluid drop on a standard SAW IDT aperture's edge as illustrated in Figure 3. Fluorescent polystyrene 1 μm particles (PolyBead Microspheres, Polysciences, Inc., Warrington, PA USA), a size less than the transition threshold to be influenced by direct acoustic forces, 5 μm, were

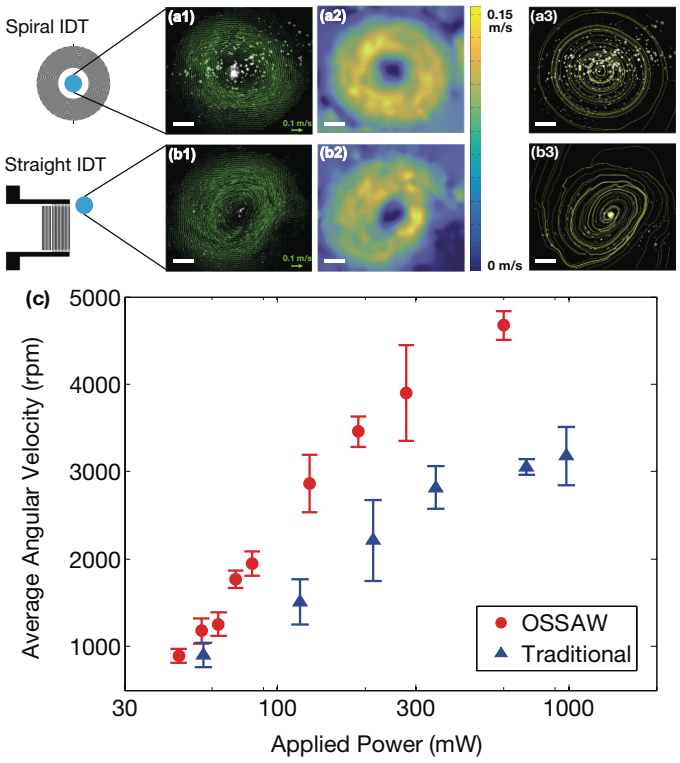

Fig. 3 A comparison between (a) OSSAW and (b) traditional offset droplet spinning using a straight IDT configuration may be made from (a1,b1) vector velocity, (a2,b2) velocity magnitude, and (a3,b3) particle streamlines for a 1.5 $\mu\ell$ DI water droplet. Average eccentricities of 0.28 and 0.81, respectively, were computed from the streamlines of (a3) the OSSAW and (b3) traditional straight IDT devices. These streamlines were calculated using PIVlab, suggesting an improved axisymmetric droplet spinning via OSSAW. (c) The OSSAW also produces a greater average angular velocity (rpm) for a given applied power. The maximum possible rotation speed from the traditional design at any power is 3180 rpm; the droplet is ejected from the surface at greater input powers. However, with OSSAW, a speed of 4670 rpm may be achieved, at which point atomization begins to appear. The error bars represent the standard deviation ($n = 5$ for each data point).

mixed into a deionized (DI) water suspension for tracking acoustic streaming immediately prior to placing a 1.5 $\mu\ell$ fluid drop of the suspension onto the OSSAW device (Fig. 3a). Due to the hydrophilicity in the central region and the hydrophobicity outside it, the droplet remains in the hydrophilic region, the center of the OSSAW device. A similar approach was used for the traditional SAW droplet concentrator configuration with straight IDTs as a benchmark control (Fig. 3b). The concentration of the particles was 4×10^9 particles/mℓ, chosen for ease of visualization and particle tracking. The effect of concentration on the behavior of acoustofluidic concentration and separation is weak and has been explored in past work[1].

Microparticle image velocimetry (μPIV) was performed while viewing the sessile drop from above, using a high-speed camera (at 500 fps, K2 DistaMax lens, Infinity Optical, Centennial, CO USA and Fastcam Mini UX, Photron, San Diego, CA USA). We used an open-access PIV analysis tool (PIVlab)[37]. This tool is able to track visible fluorescence particles and accommodates appearance and disappearance of particles from the view due to the edges, migration from the focal plane and towards or away from the objective lens (i.e., out of focus), or superposition from the camera's perspective. This method of PIV is sometimes called "poor-man's PIV" because it does not require special two-shot rapid laser illumination. Instead, the PIV is computed from individual and equally spaced frames of the video taken at 500 fps.

We set the variable zoom, long working distance microscope lens at 5X magnification to ensure the depth of field is larger than the depth of the droplet and the field of view is larger than the drop size. This prevents particle loss or gain in the video. The radial position and circumferential velocity of all visible particles, well over 1000 per experiment, were determined by the software after manually identifying the center of rotation and representing the droplet as a circulating vortex. In our experiments, this was consistently at the center of the drop. The radial velocity is computed but not used. Some—fewer than 5% in each run—of the particles are adherent on the substrate or clearly adjacent the substrate, and these are ignored by retaining the velocities of only those particles that exhibit a circumferential velocity greater than 10% of the mean circumferential velocity of all the observed particles. The angular velocity of each of the remaining particles was determined by its circumferential velocity divided by its radial distance from the drop center, and the average angular velocity was then calculated. The error bars represent the standard deviation of all of the points over five distinct runs, each with a fresh droplet run in the system.

From the μPIV velocity and streamline plots in Fig. 3a-c, the OSSAW device clearly produces a more axisymmetric streaming pattern in the sessile drop than the traditional offset design. To quantify this for the reader, consider the eccentricity of the streamlines traced out by the particles as the flow rotates in the drop (*see* Fig. 3(a3, b3)); an eccentricity of zero is ideal, representing a circular path, while an eccentricity of one is a line. With OSSAW, the average eccentricity of the streamlines is 0.28, substantially more "circular" than an eccentricity of 0.81 from a traditional straight IDT-based design. The distortion in the traditional approach has long been known to lead to instability that limits its maximum rotation speed[25]. The OSSAW provides uniform energy input, reducing interfacial deformation due to asymmetry in the acoustic streaming that can grow to eject the droplet. While other methods have been proposed to spin droplets using straight and curved IDT structures[25], fundamentally those approaches do not offer the symmetry of incident SAW provided by OSSAW.

Further, the OSSAW produces greater rotation speed at the same applied power, and can perform fluid spinning up to about 4600 rpm, representing about ~10 g (98.7 m/s^2) of acceleration (Fig. 3(c)). This limit is defined by the appearance of atomization from the drop surface. Nearly uniform throughout, the drop rotation speed is 59% faster on average per unit power for the OSSAW device versus the traditional approach. It is important to note the presence of an Ekman layer adjacent the substrate of about 50 μm in depth,[38] and in this region the flow is slower, as it is with all acoustofluidic devices.

4 Size-based particle separation via OSSAW

4.1 Separation mechanism

OSSAW appears to concentrate larger objects at the center of the droplet and smaller objects at the periphery, consistent with other sessile drop rotation devices from the past[20,21,38]. As the dominant force at the length scale of objects greater than a threshold particle size, R_{th}, the acoustic radiation force overwhelms the radial inertia due to centripetal acceleration, often and erroneously referred to as *centrifugal forces*. Taking a balance between the acoustic radiation force and the centripetal acceleration-induced radial force, it becomes possible to determine this threshold particle size. Based on analysis from King[31] and later Doinikov[32] concerning the acoustic radiation pressure on a sphere in a plane progressive wave,

$$F_{AR} = 2\pi\rho_f \frac{(2\pi f)^4}{c_f^6} R^6 \dot{\xi}^2 \frac{1+\frac{2}{9}(1-\frac{\rho_f}{\rho_p})^2}{(2+\frac{\rho_f}{\rho_p})^2} \propto R^6 \tag{4}$$

for $fR/c_{SAW} \ll 1$, where ρ_p is the particle density, f is the frequency of the acoustic wave, c_f is the sound velocity in fluid medium, R is the particle radius, and $|\dot{\xi}|$ is the fluid particle velocity. The radial force produced by their inertia in countering the centripetal acceleration that would be required for them to follow the circular path as the drop spins may be depicted as

$$F_c = \omega^2 r(\rho_p - \rho_f)\frac{4}{3}\pi R^3 \propto R^3, \tag{5}$$

where ω is the instantaneous angular velocity of the particle and r is the instantaneous radius of the particle trajectory. When the particle's radius R is large relative to the threshold R_{th} defined by the equality of $F_{\text{AR}} = F_c$,

$$R_{\text{th}}^3 = \left(\frac{r\omega^2 c_f^6}{24\pi^4 f^4 \dot{\xi}^2}\right) \frac{(\rho_f - \rho_p)\left(2+\frac{\rho_f}{\rho_p}\right)^2}{\rho_f\left(1-\frac{\rho_f}{\rho_p}\right)^2}, \tag{6}$$

the acoustic radiation force overwhelms the inertial motion of the particles. Because of the strongly nonlinear sixth-order dependence of F_{AR} upon R in eqn. (4), the transition from acoustic radiation force-dominated particle motion to motion governed by the hydrodynamics as the particle size increases is very rapid. Particles smaller than the threshold R_{th} will radially cross streamlines to the periphery of the drop due to their inertia—if the OSSAW is sufficiently powerful to cause the particles' inertia to be significant in comparison to other local effects such as shear migration.

It is perhaps best noted here that the *direction* of the acoustic force is not oriented radially to exactly oppose centripetal acceleration-induced particle motion. In our configuration, it is oriented $\alpha = 22.5^\circ$ from the radial direction, implying the equality between the radial force due to the acoustic wave and the centripetal acceleration is instead $F_{\text{AR}}\cos\alpha = F_c$, and so the particle size threshold would become $R'_{\text{th}} = \sqrt[3]{1/\cos\alpha}\,R_{\text{th}}$. But notice that $\sqrt[3]{1/\cos\alpha} \approx 1.027$, very nearly one, and so the effect is negligible. If the reader chooses, however, to orient the acoustic wave from the IDT such that α is much larger, this effect may be important to consider.

In principle, it is straightforward to identify the appropriate frequency to set the threshold particle radius R_{th} to produce significant acoustic forces on particles larger than the threshold that are nearly absent on particles smaller than this threshold. But this is true only if the sessile drop rotation velocity, ω is always the same. When switching from water to blood, for example, the viscosity changes as well, and this affects the drop's rotation velocity. One could try to compensate by changing the input power, which changes the droplet rotation speed, ω. However, this will also change the particle velocity in the fluid $|\dot{\xi}|$. Careful study of eqn. (6) shows that $R_{\text{th}}^3 \sim \omega^2/\dot{\xi}^2 \sim P_{\text{in}}/P_{\text{in}} \sim 1$, where P_{in} is the input power, implying that the threshold particle size is not dependent upon the power input. This arises because $\omega^2 \sim P_{\text{in}}$ from Fig. 3 (to a coefficient of determination $R^2 \approx 0.9$)—as expected because the square of the streaming velocity scales with the input power—and $\dot{\xi}^2 \sim P_{\text{in}}$ from numerous places in the literature[2].

Consider two cases, the first polystyrene particles in water, and the second murine blood cells in plasma, diluted to 6% hematocrit. These two cases are tested later, but let us consider what would be appropriate here in the context of frequency selection. Suppose we wish to separate 1 μm PS particles in water from larger PS particles. It is possible to spin a 1.5 $\mu\ell$ droplet of water at $\omega = 4000$ rpm using 1 W into the OSSAW device, nearly independent of the frequency choice. At $f = 100$ MHz this would set the threshold particle size at $R_{\text{th}} = 1.23$ μm. Choosing $f = 40$ MHz gives $R_{\text{th}} = 4.17$ μm. Either choice works, but the former likely would produce more selective results.

More importantly, notice the effect of now switching to blood. Even diluted, the viscosity is significantly increased and the rotation velocity of a 1.5 $\mu\ell$ droplet of this fluid is much lower at $\omega = 1800$ rpm with the same input power, $P_{\text{in}} = 1$ W. This causes the threshold particle size to be only $R_{\text{th}} = 0.72$ μm at $f = 100$ MHz, and $R_{\text{th}} = 2.45$ μm at $f = 40$ MHz.

In reality, the desire to perform the separation as quickly as possible, paired with the need to avoid local interparticle effects that manifest over longer periods of time, encourages one to seek the fastest drop rotation speed possible for the fluid under study. While a detailed analysis is possibly instructive, it is easier to simply fabricate and test a number of devices to search for the one arrangement that produces the quickest separation results.

4.2 Multi-size particle separation

Polystyrene (PS) particles (Polysciences, Inc., Warrington, PA, USA) with diameters of 1, 5, and 43 μm were selected to demonstrate size-selective microscale separation via the OSSAW device. These particles were mixed into DI water with concentrations, respectively, of 4×10^9, 6.3×10^7, and 1×10^5 particles/mℓ as representative concentrations. As noted earlier, the effect of concentration on the behavior of acoustofluidic concentration and separation is weak and has been explored in past work[1]. A 1.5 $\mu\ell$ droplet of this suspension was immediately transferred by pipette onto the hydrophilic circular region at the center of the OSSAW device (Fig. 4a and video via ESI†). An operating frequency of 40 MHz was chosen to produce a threshold separation particle

size of $R_{th} = 4.17$ μm for $\omega = 4000$ rpm using 1 W, just slightly smaller than the intermediate PS 5 μm particle size.

After applying $\sim$1 W input power to the OSSAW device, the particles separated and concentrated at different locations in the droplet in $\sim$1 s (Fig. 4(b)). The smallest particles (1 μm), relatively unaffected by the ARF, collected at the periphery of the droplet; the intermediate particles (5 μm) collected as an annular ring in the droplet; and the largest particles (43 μm) collected at the center of the droplet. This marks the first time rings of particles have been consistently seen, and may indicate the benefit of using axisymmetric acoustic waves in manipulating the droplet and particles within. It also indicates that there is a possibility of obtaining, reliably, an intermediate result between concentration at the drop's center or edge when the particle size is approximately the same as R_{th}.

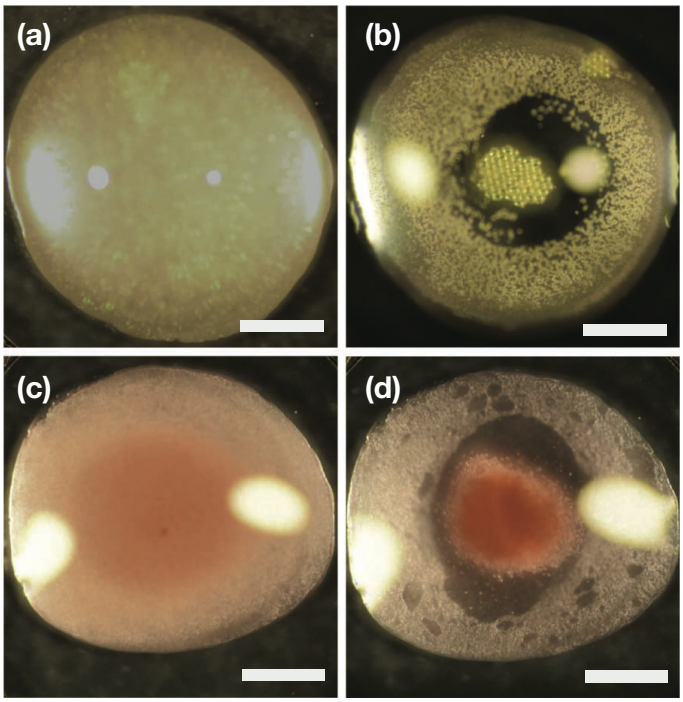

Fig. 4 A (a) 1.5 $\mu\ell$ drop with 1 μm (red), 5 μm (green), 43 μm (green) polystyrene (PS) particles randomly distributed within. (b) After OSSAW separation, showing 1 μm, 5 μm, 43 μm PS particles separated from periphery to center of the droplet. (c) 1.5 $\mu\ell$ diluted mouse blood before separation. (d) After OSSAW separation, red blood cells and the occasional white blood cell appear at the drop's center, while platelets and smaller components of blood appear at the drop's periphery The bright dots on the droplets are specular reflections of externally placed lights from the droplet surface (scale bar: 0.5 mm).

4.3 Blood cell separation

The utility of OSSAW is best examined through a potential application, and blood cell separation was considered a potential clinical use of the technology. Fresh whole blood was extracted from live mice (strain C57BL/6J, Jackson Laboratories, ME USA) and kept in an ethylenediaminetetraacetic acid-coated microtube (EDTA–K3, Becton Dickinson, Franklin Lakes, NJ USA) to prevent clotting prior to use. The blood was diluted with phosphate buffered saline (PBS) to a ratio of 1:5, representing a hematocrit of 6%, with bovine serum albumin (BSA) added (1.6% by weight). Murine red blood cells are biconcave, spherical, and about 4–7 μm in diameter, similar to human blood, and number about 7–13 $\times 10^6$ particles per $\mu\ell$ of whole blood.[39] Murine platelets, however, are smaller at 0.5 μm in diameter and are more numerous (730,000/$\mu\ell$)[40] and heterogeneous than their human counterpart (1-2 μm in diameter)[41]. White blood cells (WBCs) are rare in small blood samples.

Based on the lower drop rotation speed of $\omega = 1800$ rpm at $P_{in} = 1$ W into the OSSAW device, we selected $f = 40$ MHz to produce a separation threshold of $R_{th} = 2.45$ μm between the platelet and RBC diameters. After depositing a 1.5 $\mu\ell$-sized droplet onto the OSSAW device and operating it for 5 s, the larger cells (RBCs and WBCs, latter very rare) were found concentrated in the middle of the drop, while the platelets were found at the periphery (Fig. 4(d)).

5 Extraction and Isolation Platform

5.1 Experimental setup

An extraction platform was devised to extract separated portions of particles or blood components from the center of the droplet to perform true size-based separation and isolation for further analytical and biological analysis. As shown in Fig. 1(a,c), a 100 μm hole was drilled at the center of the OSSAW device from the back side of the LN chip using an excimer (exciplex) laser at a wavelength of 189 nm, a firing rate of 300 Hz, and an instantaneous power of 100 W for each "shot". The hole was drilled using 120 groups of ten repeated shots, refocusing the laser's focal plane into the hole between groups as it progressed by 50 μm increments (LaserShot, Optec Laser Systems, Brussels, Belgium). Glass capillary tubes, 80μm outer diameter (OD) and 50 μm inner diameter (ID), were introduced into the hole for extraction after separation (see Fig. 8(a)). A 1 mℓ syringe was attached to the glass capillary tube using hot glue (see Fig. 8(b)). The complete extraction platform is provided in Fig. 8(c), showing components necessary for system alignment, tube insertion, particle extraction, and tube extraction.

5.2 Extraction results and separation performance

The as-separated portion of the blood sample at the droplet's center was extracted from the hole using the glass capillary tube placed into the underside of the OSSAW device (Fig. 5 and video via ESI†). By contrast, the separated portion at the drop periphery was collected using a fine pipette tip from the top of the OSSAW device.

It is possible to extract samples using either method, and depending on the reader's ability to introduce holes into LN and the desired extraction workflow, one or the other choice may prove more suitable. In the latter case, with extraction from above, it is important to note that leaving the acoustic wave on as supplied from the SAW prevents cell adhesion to the substrate and consequently improves the extraction results. In extracting particles from below, this is less of a problem.

For particle separation, we discarded the 43 μm PS particles

and selected only the 1 μm and 5 μm PS particles. The larger 43 μm particles tend to clog the 50 μm extraction capillary tube. The 5 μm and 1 μm PS particles were mixed in equal numbers in the sample (i.e., the quantity ratio was 1:1), with a concentration of 4×10^5 particles/mℓ. Due to this smaller particle pair, we chose the 100 MHz OSSAW to produce $R_{\text{th}} = 1.23$ μm. This frequency is higher than the initial 56.5 MHz OSSAW device in Figs. 2 and 3 and the 40 MHz used for the PS particle and murine blood separations in Fig. 4. Separation was initially performed using the OSSAW at 1 W for 1 s on a 1.5 $\mu\ell$ fluid sample.

As-separated particles were then extracted with fluid from the center and edge, and the two extracted fluid-particle samples were analyzed using flow cytometry (Attune NxT Flow Cytometer, ThermoFisher, Waltham, MA, USA), distinguishing the particle size by forward scatter and side scatter. The numerical purity of 5 μm beads at the drop center was 83%, while the numerical purity of the 1 μm beads at the drop periphery was 97% (see Fig. 6(a,b)). Numerical purity in this context is defined by the number of target particles divided by the total number of particles in the extracted sample.

For blood cell separation, the OSSAW was operated at 1 W and a frequency of 40 MHz in order to place the separation size threshold $R_{\text{th}} = 2.45$ μm between the platelet and RBC diameters. Two 0.75 $\mu\ell$ samples were extracted from the periphery and center of a 1.5 $\mu\ell$ diluted (6% hematocrit) and OSSAW-separated mouse blood droplet were transferred into individual wells of a 96-well assay plate (Fisher Scientific, Waltham, MA, USA) with staining buffer (PBS + 1.6% BSA) to assess cell viability, perform antibody staining, and minimize non-specific binding. Antibodies targeting TER119 (Fluorescein isothiocyanate (FITC)), CD45 (Alexa Fluor 594), and CD41 (Alexa Fluor 700) (all Biolegend, San Diego, CA, USA) were used to stain RBCs, WBCs, and platelets, respectively. Incubation was performed for 30 min at 4°C in the dark after introducing the antibodies. Flow cytometry (ZE5 Cell Analyzer, Bio-Rad, Hercules, CA, USA) was then performed to identify the cell separation performance of OSSAW. As shown in Fig. 6(c,d), OSSAW isolates platelets at the drop periphery and RBCs at the drop's center with 83.8% and 92.7% numerical purity, respectively. The plot omits CD45 used to stain WBC, as the number of WBCs in 1 $\mu\ell$ samples—a few per sample—is insufficient to produce statistically valid, quantifiable results via flow cytometry. The few WBCs that do appear in a given sample are consistently extracted with the RBCs.

6 Conclusions

In this paper, we demonstrated a novel omnidirectional spiral SAW design—OSSAW—and presented the utility of efficient axisymmetric fluid spinning at up to $\sim 10g$, producing effective separation of particles and cells in a microliter drop. The maximum rotation speed of 4500 rpm is roughly twice the speed of classic configurations like the common offset straight IDTs arrangement, and OSSAW offers this advantage at lower input powers. By using OSSAW, particles of different sizes and mouse blood may each be separated. We also demonstrated the unique appearance of rings for particles of size similar to the threshold size R_{th}, suggesting a possible means to produce greater discretion in separation of mixed particle samples. The importance of considering the fluid viscosity was illustrated through a comparison of water and blood-based samples, through its effects on the drop rotation speed, not, counterintuitively, due to any changes in the acoustic phenomena.

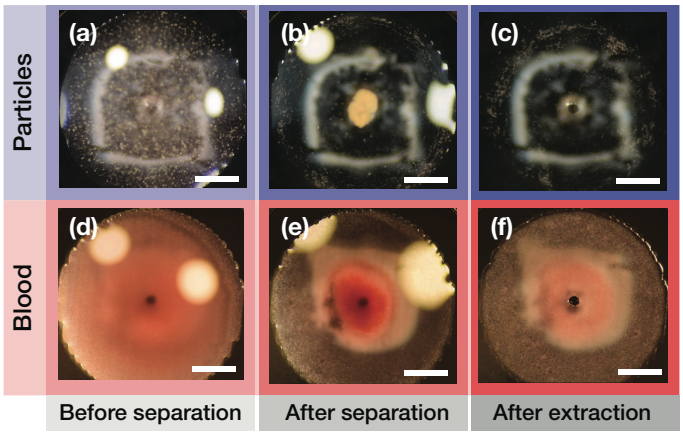

Fig. 5 (a–c) Separation and extraction of 5 μm (green) polystyrene particles from 1 μm (red) polystyrene particles in a 1.5 $\mu\ell$ DI water droplet (a) Before separation: droplet with 1 μm and 5 μm randomly distributed particles. (b) After separation: 5 μm particles concentrate in the middle of the drop, while 1 μm particles are at the periphery of the drop. (c) After extraction: 5 μm particles are extracted through a glass capillary tube from the middle hole of the device; the 1 μm particles are extracted from a pipette and glass capillary tube introduced at the drop periphery from above (not shown). (d–f) Separation and extraction of red blood cells (RBCs) from mouse blood. (d) Before separation: 1.5 $\mu\ell$ mouse blood on OSSAW device (e) After separation: RBCs concentrate in the middle of the drop, while platelets appear at the periphery. (f) RBCs are extracted via a glass capillary tube from a hole through the middle of the OSSAW device. (Scale bar: 0.5 mm.)

Furthermore, we devised an extraction platform to withdraw concentrated particle and cell samples composed of either specific particle sizes or mouse blood components after using the OSSAW, for the first time in a sessile-drop based device. The approach provides a separation purity above 80% according to flow cytometry. While these results are comparable to other separation techniques, including past SAW-based methods in Table 1, the many advantages of a surface acoustic wave-based approach—biocompatibility, fast fluidic actuation via large forces despite small scale, contact-free manipulation, on-chip integration, and flexibility in design—suggest ample opportunity for improving this approach for applications into the future.

With further work, this simple approach provides yet another acoustofluidic tool to deliver on the promise of true lab-on-a-chip diagnostics.

Acknowledgements

The authors are grateful to the University of California and the NANO3 facility at UC San Diego for provision of funds and facilities in support of this work. This work was performed in part at the San Diego Nanotechnology Infrastructure (SDNI) of UCSD, a member of the National Nanotechnology Coordinated Infrastructure, which is supported by the National Science Foundation (Grant ECCS–1542148). The work presented here was gener-

Table 1 A comparison of separation performance using SAW in microfluidics devices from the literature.

Method	Composition	Throughput	Purity	Ref.
SSAW* in channel	Beads with different densities	8-18 $\mu\ell$/min	98%	[14]
SSAW in channel	polystyrene & melamine beads	0.2-2 $\mu\ell$/min	98.8%-89.4%	[15]
SSAW in channel	platelets & RBCs	0.25-5 $\mu\ell$/min	74.1% & 99%	[16]
SSAW in channel	0.87 μm & 4.17 μm PS particles	NA	80%	[17]
TSAW† in channel	3 μm & 10 μm particles	100-300 $\mu\ell$/h	100%	[18]
TSAW in channel	10/15 μm PS and PMMA particles	1-4 $\mu\ell$/min	95%	[19]
TSAW in droplet	1, 3, 6, 20, 45 μm PS particles	5 $\mu\ell$	NA	[20]
TSAW in droplet	1 μm & 10 μm PS particles	5 $\mu\ell$	NA	[21]
FSAW‡ in droplet	6 μm & 31 μm PS particles	1.5-3 $\mu\ell$	NA	[24]
OSSAW in droplet	5 μm & 1 μm PS particles	1.5 $\mu\ell$ drop	83% & 97%	—
OSSAW in droplet	platelets & RBCs	1.5 $\mu\ell$ drop	83% & 93%	—

*SSAW is a standing SAW, †TSAW is a traveling SAW, and ‡FSAW is a focusing SAW.

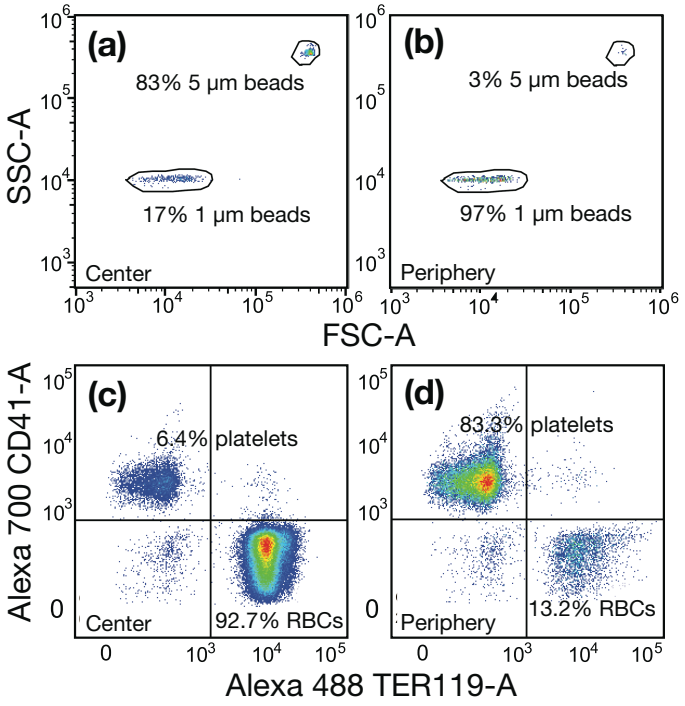

Fig. 6 Separation performance via OSSAW after separation and extraction by flow cytometry. By providing 100 MHz OSSAW into a microliter scale fluid drop, (a) 5 μm PS particles concentrate at the center, while (b) 1 μm PS particles migrate to the periphery. With diluted murine blood (6% hematocrit), 40 MHz was used instead to separate (c) murine RBCs concentrated at the drop's center, while (d) murine platelets migrated to the periphery.

ously supported by a research grant from the W.M. Keck Foundation. The authors are also grateful for the support of this work by the Office of Naval Research (via Grant 12368098), and substantial technical support by Polytec's staff in Irvine, CA and Waldbronn, Germany.

7 Appendix

7.1 Derivation of the equation to describe the OSSAW IDT finger pattern

The derivation of the equation to describe a spiral pattern for the OSSAW's interdigital transducer (IDT) finger electrodes is provided as follows, referring to Fig. 1(b). It is important to note here that, to our knowledge, this spiral structure is not represented by a defined spiral from the literature. It is neither an Archimedian spiral of $r = a + b\theta$, Fermat spiral $r = a\sqrt{\theta}$, nor a Doyle spiral $r = \theta + \sqrt{\theta}$.

Using polar coordinates (r,θ) with unit vectors $\mathbf{e}_r$ and $\mathbf{e}_\theta$ in a standard right-handed coordinate system with $\mathbf{e}_z$ pointing towards the reader, we seek to generate SAW from every point on the IDT to propagate into the inner $r \le R_2$ region such that the SAW is always tangent to a circle of radius R_0. Due to circular symmetry, we restrict our consideration to one spiral finger, and enforce the condition $r(\theta = 0) = R_1$. The position vector for a point, B, somewhere on a finger of the spiral IDT as defined from the center, O, is $\mathbf{r} = r(\theta)\mathbf{e}_r$, with $r(\theta)$ indicating that the radial position r explicitly depends on the azimuthal angle θ. Note that $\mathbf{e}_r$ serves as the unit vector along the coordinate direction θ. Taking a time derivative of this vector produces the "velocity" of the point B,

$$\frac{d\mathbf{r}}{dt} = \dot{r}\,\mathbf{e}_r + r\dot{\theta}\,\mathbf{e}_\theta, \tag{7}$$

where the dots over r and θ are shorthand for a time derivative. Of course the point B is not moving, but this helpfully indicates the tangent direction to the IDT finger, $\mathbf{e}_t = \dot{\mathbf{r}}/|\dot{\mathbf{r}}|$. The inward-propagating SAW travels, therefore, from B in a direction perpendicular to $\mathbf{e}_t$, along $\mathbf{e}_{\text{SAW}} = \mathbf{e}_z \times \mathbf{e}_t$. Explicitly writing $\mathbf{e}_{\text{SAW}}$ in terms of the orthogonal unit vectors $\mathbf{e}_r$ and $\mathbf{e}_\theta$, we find

$$\mathbf{e}_{\text{SAW}} = -\cos\gamma\,\mathbf{e}_r + \sin\gamma\,\mathbf{e}_\theta. \tag{8}$$

We may also write from eqn. (7)

$$\mathbf{e}_{\text{SAW}} = \mathbf{e}_z \times \frac{\dot{\mathbf{r}}}{|\dot{\mathbf{r}}|} = \mathbf{e}_z \times \left(\frac{\dot{r}\mathbf{e}_r}{\sqrt{\dot{r}^2 + r^2\dot{\theta}^2}} + \frac{r\dot{\theta}\mathbf{e}_\theta}{\sqrt{\dot{r}^2 + r^2\dot{\theta}^2}} \right), \tag{9}$$

producing

$$\mathbf{e}_{\text{SAW}} = \frac{-r\frac{d\theta}{dt}\mathbf{e}_r + \frac{dr}{d\theta}\frac{d\theta}{dt}\mathbf{e}_\theta}{\sqrt{\left(\frac{dr}{d\theta}\frac{d\theta}{dt}\right)^2 + r^2\left(\frac{d\theta}{dt}\right)^2}} = \frac{-r\mathbf{e}_r + r'\mathbf{e}_\theta}{\sqrt{(r')^2 + r^2}}, \tag{10}$$

by eliminating $d\theta/dt$ and defining $r' = dr/d\theta$.

Note that $\sin\gamma = \overline{OA}/\overline{OB} = R_0/r$. Using this and equating like terms from eqns. (8) and (10) along the $\mathbf{e}_\theta$ direction by using

$\mathbf{e}_\theta \cdot \mathbf{e}_{\mathrm{SAW}}$ for both expressions, we find

$$\sin\gamma = \frac{r'}{\sqrt{(r')^2 + r^2}} = \frac{R_0}{r}, \tag{11}$$

producing, with a little algebra,

$$d\theta = \sqrt{\frac{1}{R_0^2} - \frac{1}{r^2}}\, dr. \tag{12}$$

Equation (12) is an ordinary differential equation that relates r and θ. We integrate it from $(r,\theta) = (R_1, 0)$ to (r,θ), producing

$$\begin{aligned}\theta &= \int_{R_1}^{r} \sqrt{\frac{1}{R_0^2} - \xi^{-2}}\, d\xi \\ &= \sqrt{\frac{r^2}{R_0^2} - 1} - \tan^{-1}\sqrt{\frac{r^2}{R_0^2} - 1} - \sqrt{\frac{R_1^2}{R_0^2} - 1} + \tan^{-1}\sqrt{\frac{R_1^2}{R_0^2} - 1}.\end{aligned} \tag{13}$$

This expression relating the radial coordinate r to the azimuthal coordinate θ may then be used to produce the spiral IDT of the OSSAW, as explained in the main text.

7.2 Extraction platform with OSSAW

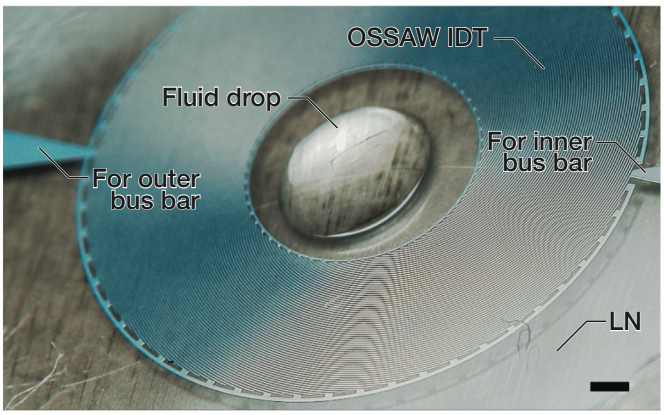

Fig. 7 A 56.5 MHz OSSAW device with a microliter sessile drop on the inner circular region, showing the fingers and electrode connection to produce a suitable spiral SAW. The connection to the inner bus bar is via a single finger in this particular design to preserve the IDT design (at right: for inner bus bar), while the connection to the outer bus bar is at left. This device lacks the central extraction hole. (Scale bar: 0.5 mm.)

Fig. 7 is a photograph of a functioning OSSAW device with a deionized water droplet placed at the center, while Fig. 8 illustrates the basic procedure for fabricating and testing the OSSAW concentration and extraction devices.

7.3 Detailed protocol for antibody-stained mouse blood cell flow cytometry

The separated portions of blood samples were first transferred into a 96-well, V-bottom plate (Sigma-Aldrich, St. Louis, MO, USA) with 100 $\mu\ell$ phosphate-buffered saline (PBS, 1X, pH 7.4, Thermo Fisher Scientific, Waltham, MA, USA) and 1.6% bovine

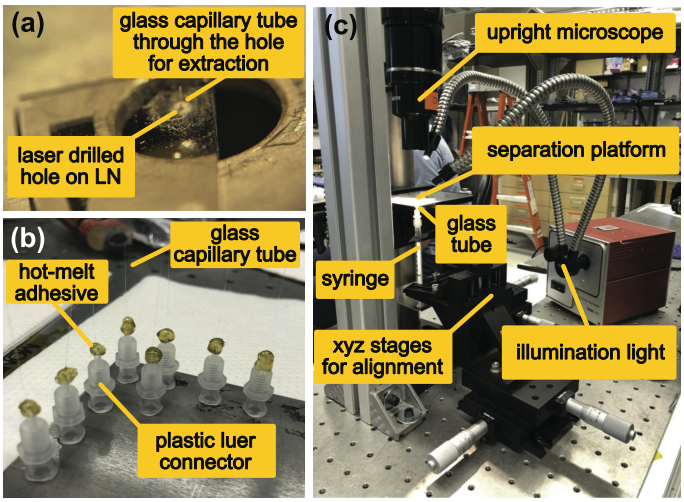

Fig. 8 (a) An 80 μm outer diameter glass capillary tube is inserted into a 100 μm diameter hole in LN substrate for the extraction platform. (b) A luer lock connector is attached to the glass capillary tube using hot-melt adhesive to facilitate syringe attachment. (c) Image of the extraction platform, including lab-based components for system alignment.

serum albumin (BSA, Thermo Fisher Scientific, Waltham, MA, USA). Antibodies conjugated with red blood cells (RBC, FITC anti-mouse TER-119/Erythroid Cells Antibody, Biolegend, San Diego, CA, USA), white blood cells (WBC, Alexa Fluor® 594 anti-mouse CD45 Antibody, Biolegend, San Diego, CA, USA), and platelets (Alexa Fluor® 700 anti-mouse CD41 Antibody, Biolegend, San Diego, CA, USA) were added into subsequent wells, each with a volume of 0.5 $\mu\ell$, 0.1 $\mu\ell$, and 0.2 $\mu\ell$, respectively. The samples were then incubated at 4 °C for 30 min in the dark. The 96-well plate was centrifuged at 500g for 5 min. Supernatant was extracted from the centrifuged samples. Another 100 $\mu\ell$ fresh PBS with 1.6% BSA was added and resuspended in each well. The sample was centrifuged and washed for a second time with the same procedure as described above.

The samples were finally analyzed via flow cytometry (ZE5 Cell Analyzer, Bio-Rad, Hercules, CA, USA and Attune NxT Flow Cytometer, ThermoFisher, Waltham, MA, USA). The results of processing a blood sample without using the SAW is provided in Fig. 9 to provide a basis for comparing the effects of OSSAW-driven cell separation. The plot omits CD45 used to stain WBC, as the number of WBCs in a 1 $\mu\ell$ sample is insufficient to produce statistically valid, quantifiable results via flow cytometry. The composition of the sample without OSSAW-driven separation is 72.9% RBC and 26.1% platelets.

Notes and references

1 W. Connacher, N. Zhang, A. Huang, J. Mei, S. Zhang, T. Gopesh and J. Friend, *Lab on a Chip*, 2018, **18**, 1952–1996.

2 J. Friend and L. Y. Yeo, *Reviews of Modern Physics*, 2011, **83**, 647.

3 X. Ding, P. Li, S.-C. S. Lin, Z. S. Stratton, N. Nama, F. Guo, D. Slotcavage, X. Mao, J. Shi, F. Costanzo *et al.*, *Lab on a Chip*, 2013, **13**, 3626–3649.

4 P. Zhang, H. Bachman, A. Ozcelik and T. J. Huang, *Annual*

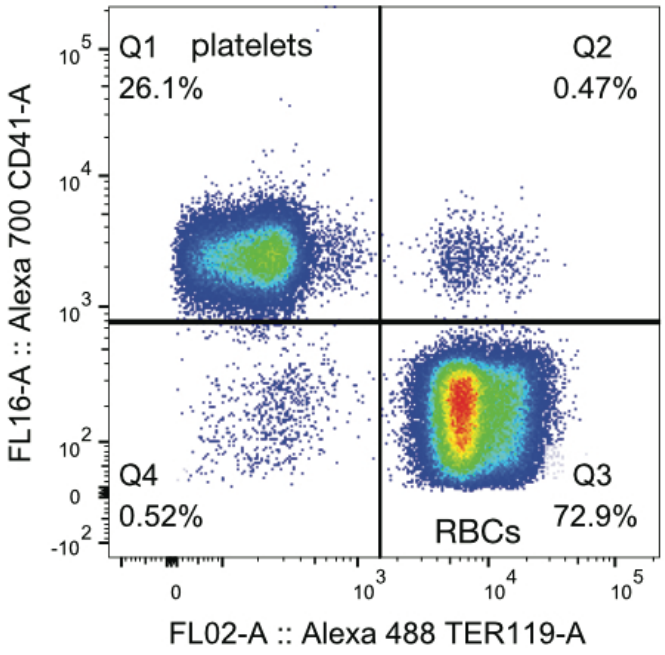

Fig. 9 Flow cytometry on an unseparated (no OSSAW) blood sample that is otherwise identical to those used for OSSAW separation in Fig. 6. The composition of the sample is 72.9% RBC and 26.1% platelets. Though CD45 was used for WBC detection, the number of WBC in these 1 $\mu\ell$ blood samples was too low to justify their display here or in Fig. 6.

Review of Analytical Chemistry, 2020, **13**, 17–43.

5 A. Ozcelik, J. Rufo, F. Guo, Y. Gu, P. Li, J. Lata and T. J. Huang, *Nature methods*, 2018, **15**, 1021–1028.

6 Z. Tian, S. Yang, P.-H. Huang, Z. Wang, P. Zhang, Y. Gu, H. Bachman, C. Chen, M. Wu, Y. Xie *et al.*, *Science advances*, 2019, **5**, eaau6062.

7 J. Lighthill, *Journal of Sound and Vibration*, 1978, **61**, 391–418.

8 T. Uchida, T. Suzuki and S. Shiokawa, Ultrasonics Symposium, 1995. Proceedings., 1995 IEEE, 1995, pp. 1081–1084.

9 M. B. Dentry, L. Y. Yeo and J. R. Friend, *Physical Review E*, 2014, **89**, 013203.

10 S.-C. S. Lin, X. Mao and T. J. Huang, *Lab on a Chip*, 2012, **12**, 2766–2770.

11 C. W. Shields IV, C. D. Reyes and G. P. López, *Lab on a Chip*, 2015, **15**, 1230–1249.

12 A. Lenshof, C. Magnusson and T. Laurell, *Lab on a Chip*, 2012, **12**, 1210–1223.

13 D. J. Collins, B. L. Khoo, Z. Ma, A. Winkler, R. Weser, H. Schmidt, J. Han and Y. Ai, *Lab on a Chip*, 2017, **17**, 1769–1777.

14 J. Nam, H. Lim, C. Kim, J. Yoon Kang and S. Shin, *Biomicrofluidics*, 2012, **6**, 024120.

15 M. C. Jo and R. Guldiken, *Sensors and Actuators A: Physical*, 2012, **187**, 22–28.

16 J. Nam, H. Lim, D. Kim and S. Shin, *Lab on a Chip*, 2011, **11**, 3361–3364.

17 J. Shi, H. Huang, Z. Stratton, Y. Huang and T. J. Huang, *Lab on a Chip*, 2009, **9**, 3354–3359.

18 G. Destgeer, K. H. Lee, J. H. Jung, A. Alazzam and H. J. Sung, *Lab on a Chip*, 2013, **13**, 4210–4216.

19 Z. Ma, D. J. Collins, J. Guo and Y. Ai, *Analytical Chemistry*, 2016, **88**, 11844–11851.

20 H. Li, J. R. Friend and L. Y. Yeo, *Biomedical Microdevices*, 2007, **9**, 647–656.

21 G. Destgeer, H. Cho, B. H. Ha, J. H. Jung, J. Park and H. J. Sung, *Lab on a Chip*, 2016, **16**, 660–667.

22 R. P. Hodgson, M. Tan, L. Yeo and J. Friend, *Applied Physics Letters*, 2009, **94**, 024102.

23 Y. Bourquin, A. Syed, J. Reboud, L. C. Ranford-Cartwright, M. P. Barrett and J. M. Cooper, *Angewandte Chemie International Edition*, 2014, **53**, 5587–5590.

24 P. R. Rogers, J. R. Friend and L. Y. Yeo, *Lab on a Chip*, 2010, **10**, 2979–2985.

25 R. Shilton, M. K. Tan, L. Y. Yeo and J. R. Friend, *Journal of Applied Physics*, 2008, **104**, 014910.

26 V. Laude, D. Gérard, N. Khelfaoui, C. F. Jerez-Hanckes, S. Benchabane and A. Khelif, *Applied Physics Letters*, 2008, **92**, 094104.

27 M. Baudoin and J.-L. Thomas, *Annual Review of Fluid Mechanics*, 2020, **52**, 205–234.

28 F. S. Hickernell, *Proceedings of the IEEE*, 1976, **64**, 631–635.

29 G. Bu, D. Ciplys, M. Shur, L. Schowalter, S. Schujman and R. Gaska, *Applied physics letters*, 2004, **84**, 4611–4613.

30 N. Zhang, J. Mei, T. Gopesh and J. Friend, *IEEE Transactions on Ultrasonics, Ferroelectrics, and Frequency Control*, 2020, **67**, 2176–2186.

31 L. V. King *et al.*, *Proc. R. Soc. Lond. A*, 1934, **147**, 212–240.

32 A. Doinikov, *Proceedings of the Royal Society of London. Series A: Mathematical and Physical Sciences*, 1994, **447**, 447–466.

33 F. Nadal and E. Lauga, *Physics of Fluids*, 2014, **26**, 082001.

34 J. Mei, N. Zhang and J. Friend, *JoVE (Journal of Visualized Experiments)*, 2020, e61013.

35 N. Zhang and J. Friend, *JoVE (Journal of Visualized Experiments)*, 2020, e60648.

36 A. R. Rezk, L. Y. Yeo and J. R. Friend, *Langmuir*, 2014, **30**, 11243–11247.

37 W. Thielicke and E. Stamhuis, *Journal of Open Research Software*, 2014, **2**, e30.

38 Y. Kurashina, K. Takemura and J. Friend, *Lab on a Chip*, 2017, **17**, 876–886.

39 K. E. O'Connell, A. M. Mikkola, A. M. Stepanek, A. Vernet, C. D. Hall, C. C. Sun, E. Yildirim, J. F. Staropoli, J. T. Lee and D. E. Brown, *Comparative medicine*, 2015, **65**, 96–113.

40 D. J. Walther, J.-U. Peter, S. Winter, M. Höltje, N. Paulmann, M. Grohmann, J. Vowinckel, V. Alamo-Bethencourt, C. S. Wilhelm, G. Ahnert-Hilger and M. Bader, *Cell*, 2003, **115**, 851–862.

41 A. Schmitt, J. Guichard, J. M. Massé, N. Debili and E. M. Cramer, *Exp Hematol*, 2001, **29**, 1295–1302.